Nuclear Medicine and Biology 41 (2014) e75–e83

Contents lists available at ScienceDirect

Nuclear Medicine and Biology

journal homepage: www.elsevier.com/locate/nucmedbio

DNA damage-centered signaling pathways are effectively activated during low dose-rate Auger radioimmunotherapy

Bérengère Piron [a,b,c,d,1], Salomé Paillas [a,b,c,d,1], Vincent Boudousq [a,b,c,d], André Pèlegrin [a,b,c,d], Caroline Bascoul-Mollevi [d], Nicolas Chouin [e], Isabelle Navarro-Teulon [a,b,c,d], Jean-Pierre Pouget [a,b,c,d,*]

[a] IRCM, Institut de Recherche en Cancérologie de Montpellier, Montpellier, F-34298, France
[b] INSERM, U896, Montpellier, F-34298, France
[c] Université Montpellier 1, Montpellier, F-34298, France
[d] Institut régional de Cancérologie de Montpellier, Montpellier, F-34298, France
[e] LUNAM Université, Oniris, «AMaROC», Nantes, F-44307, France

ARTICLE INFO

Article history:
Received 30 September 2013
Received in revised form 23 January 2014
Accepted 30 January 2014

Keywords:
Radioimmunotherapy
Auger electrons
Signaling pathways
DNA damage
^{125}I-mAbs

ABSTRACT

Introduction: Low dose-rate radioimmunotherapy (RIT) using ^{125}I-labelled monoclonal antibodies (^{125}I-mAbs) is associated with unexpected high cytotoxicity per Gy.
Methods: We investigated whether this hypersensitivity was due to lack of detection of DNA damage by the targeted cells. DNA damage was measured with the alkaline comet assay, gamma-H2AX foci and the micronucleus test in $p53^{-/-}$ and $p53^{+/+}$ HCT116 cells exposed to increasing activities of internalizing anti-HER1 ^{125}I-mAbs or non-internalizing anti-CEA ^{125}I-mAbs. The expression of proteins involved in radiation response and progression of cells through the cycle were determined.
Results: Cell hypersensitivity to low absorbed doses of anti-CEA ^{125}I-mAbs was not due to defect in DNA damage detection, since ATM (ataxia telangiectasia mutated gene), gamma-H2AX, p53 and p21 were activated in RIT-treated HCT116 cells and G2/M cell cycle arrest was observed. Moreover, the alkaline comet assay showed that DNA breaks accumulated when cells were placed at 4 °C during exposure but were repaired under standard RIT conditions (37 °C), suggesting that lesions detected under alkaline conditions (mostly DNA single strand breaks and alkali-labile sites) are efficiently repaired in treated cells. The level of gamma-H2AX protein corroborated by the level of foci measured in nuclei of treated cells was shown to accumulate with time thereby suggesting the continuous presence of DNA double strand breaks. This was accompanied by the formation of micronuclei.
Conclusion: Hypersensitivity to non-internalizing ^{125}I-mAbs is not due to lack of detection of DNA damage after low absorbed dose-rates. However, DNA double strand breaks accumulate in cells exposed both to internalizing and non-internalizing ^{125}I-mAbs and lead to micronuclei formation. These results suggest impairment in DNA double strand breaks repair after low absorbed doses of ^{125}I-mAbs.

1. Introduction

Auger electrons are produced in cascades during electronic shell rearrangement consecutive to electronic capture and/or conversion processes in unstable atoms [1]. They have a very low energy (from a few eV to a few keV) and are considered as high LET particles (from 4 to 26 keV/μm) when their energy is less than 1 keV. Consequently, their path length in biological matter is very short, between about 2 nm and 500 nm for most of them (for reviews see [2–8]). Due to their physical characteristics, efforts have been done to bring Auger electrons in the cell nucleus to obtain the highest cytotoxicity (for review [5]).

However, although clinical radioimmunotherapy (RIT) studies using Auger electrons labeled to monoclonal antibodies (mAbs) have not given clear-cut results [9–12], we and others have shown that, in mice, Auger electrons could efficiently delay growth of small solid tumors [13–18]. This efficacy remains to be elucidated because the final localization of ^{125}I-mAbs (and the subsequent energy deposit [19]) upon binding to their receptors is the cell membrane (non-internalizing mAbs) or the cytoplasm (internalizing mAbs) after a receptor-mediated internalizing process. Therefore, for both types of mAbs, most of the energy is released in extra-nuclear compartments. Moreover, we previously reported in several cell lines that non-internalizing ^{125}I-mAbs are more toxic than internalizing ^{125}I-mAbs

* Corresponding author at: Institut de Recherche en Cancérologie de Montpellier, Institut régional de Cancérologie de Montpellier, 34298 Montpellier Cedex 5, France. Tel.: +33 625686085.
E-mail address: jean-pierre.pouget@inserm.fr (J.-P. Pouget).
[1] Authors participated equally.

0969-8051 © 2014 Elsevier Inc. Open access under CC BY-NC-ND license.
http://dx.doi.org/10.1016/j.nucmedbio.2014.01.012

[19,20]. This higher cytotoxicity is p53-independent (differently from internalizing ^{125}I-mAbs) and does not involve cell membrane-mediated apoptotic mechanisms [19].

In conventional external beam radiation therapy (CEBRT), the nucleus is the key target of ionizing irradiation. However, the comparison between CEBRT and RIT is not straightforward. Indeed, CEBRT delivers high radiation doses (between 40 and 80 Gy) at high dose-rate (1–2 Gy.min^{-1}) that are fractionated in daily 2 Gy doses and the biological response to CEBRT is correlated with both dose and dose-rate [21,22]. The cell response to radiation is mostly triggered by DNA double strand breaks (DSBs) the occurrence of which is strictly proportional to the mean nucleus absorbed dose [21]. DSBs initiate different signaling pathways that involve ATM, a DNA damage sensor molecule. In turn, ATM activates proteins (particularly, H2AX and p53) that participate in cell cycle arrest, apoptosis and DNA repair (for reviews see [23–26]). Conversely, RIT is characterized by protracted exposure (hours to days), resulting in low total doses (10–30 Gy compared to 40–80 Gy in EBRT) delivered at low dose-rates (<1Gy.h^{-1}), and is accompanied by a strong heterogeneity in subcellular energy deposits. These physical features provide cancer cells with an opportunity for DNA repair during RIT. However, several studies in mice have shown that RIT cytotoxicity per unit of absorbed dose is higher than that of a single fraction of radiation delivered at higher dose-rate in CEBRT [27,28]. Hypotheses have been proposed for explaining such increased efficacy per Gy (for review [29]).

Here, we investigated whether the higher RIT cytotoxicity per unit of absorbed dose was due to lack of detection of DNA damage induced by low dose-rate RIT in $p53^{-/-}$ and $p53^{+/+}$ HCT116 cells targeted with ^{125}I-mAbs.

2. Materials and methods

2.1. Cell lines

HCT116 ($p53^{+/+}$) human colorectal cancer cells were from ATCC. The $p53^{-/-}$ HCT116 cell line was a gift from Professor Bert Vogelstein (Johns Hopkins University). HCT116 cells express HER1 and basal level of CEA receptors. They were grown in RPMI supplemented with 10% heat-inactivated FBS, 100 μg/mL L-glutamine and antibiotics (0.1 unit/mL penicillin and 100 μg/mL streptomycin). A-431 and SK-OV-3 cells were previously described in Ref. [20].

2.2. Antibodies and radiolabelling

The internalizing m225 mAb [19,20] was used for targeting the epidermal growth factor receptor (EGFR/HER1) expressed in HCT116 and A-431 cells. The internalizing trastuzumab (Herceptin®, Genentech Incorporated, San Francisco, CA, USA) binds to Epidermal Receptor type 2 (HER2) expressed in SK-OV-3 cells [20] and the non-internalizing murine IgG1k mAb 35A7 targets CEA in all the cell lines [19,20]. The non-targeting IgG1 mAb PX was used as control [19,20]. MAbs were radiolabelled with ^{125}I using the conventional IODO-GEN method (1,3,4,6-tetrachloro-3α, 6α-diphenylglycoluryl) described in Ref. [20].

2.3. Cellular dosimetry

The mean nucleus absorbed dose was previously calculated for HCT116 cells exposed to increasing activities (0–4 MBq/ml) of ^{125}I-mAbs [19]. Briefly, the MIRD cellular approach [30] that requires the determination of the total cumulative number of decays ($\tilde{A}_{rs}$) occurring in cells and the *S*-values was used. Then, for each test activity, radioactivity uptake per cell (Bq/cell) was determined as described in [20] and used to estimate $\tilde{A}_{rs}$. For all targeting models, $\tilde{A}_{rs}$ was then multiplied by the corresponding *S*-value to obtain the mean nucleus absorbed dose. For *S*-value calculations, three sources of irradiation were considered: self-irradiation from radiolabelled vectors that were internalized in the cytoplasm (anti-HER1 ^{125}I-mAbs) or bound to the cell membrane (anti-CEA ^{125}I-mAbs); culture medium irradiation from unbound radiolabelled vectors; and cross-fire irradiation. Cell size was measured by fluorescence microscopy after propidium iodide staining and the cell radius (distributed normally within the HCT116 cell population) was 5.6 ± 1.0 μm when the nucleo-cytoplasmic ratio was about 0.65. The cellular radioactivity was assumed to be uniformly distributed within cytoplasm and at cell surface for internalizing and non-internalizing ^{125}I-mAbs, respectively.

2.4. Alkaline single-cell gel electrophoresis

The alkaline single-cell gel electrophoresis assay (comet assay) was used to measure DNA damage in 3 × 10^5 HCT116 cells grown in 6-well plates and exposed to 0 and 4 MBq/mL of ^{125}I-mAbs. The comet assay was carried out either i) under standard RIT conditions (i.e., cells at 37 °C for the entire RIT duration) at different time points (15 min, 1 h, 2 h, 3 h, 6 h, 12 h, 24 h and 48 h), or ii) following pre-incubation of cells in cold medium at 4 °C for 1 h and RIT at 4 °C for 4 h. Samples were collected at 15 min, 30 min, 1 h, 2 h, 3 h and 4 h after RIT onset. For both conditions (37 °C and 4 °C), the methodology described in [31] was used. The tail moment (TM) was the parameter retained for analysis. The mean TM, expressed in arbitrary units (a.u.), was measured in 100 randomly chosen cells per slide for each time point and was calculated with the Comet Imager 2.0 software (Metasystems, Hamburg, Germany). Three slides for each condition and each time point were analyzed per experiment and experiments were repeated three times.

2.5. Micronucleus assay

3 × 10^4 HCT116 cells were seeded in 24-well plates. HCT116 cells exposed to activities between 0 and 4 MBq/mL of ^{125}I-mAbs for 2 days. Twenty-four hours before selected time points (day 1, day 2 and 3 post onset of RIT), cytochalasin B was added to the culture medium at a final concentration of 5 μg/mL in order to block cytokinesis and was maintained for 24 hours. Cells were then harvested and centrifuged. Supernatant was carefully discarded and the pellet was treated with KCl 125 mM under constant shaking for hypotonic chock. Cells were then fixed three times in acetic acid: ethanol (1:6), dropped onto slides under humidified atmosphere and air dried. Before analysis, slides were stained with propidium iodide (500 μg/mL). Experiments were repeated three times in triplicate.

2.6. Protein extraction and Western blotting

5 × 10^5 HCT116 and 4 × 10^5 A-431 and SK-OV-3 cells were grown in 6-well plates and exposed to 0 and 4 MBq/mL of ^{125}I-mAbs for 2 days. Proteins were extracted as described in [19]. Membranes were pre-incubated with 5% milk in PBS/0.1% Tween 20 and then with anti-p53 (1:10,000), -p21 (1:500) (Santa Cruz Biotechnology, CA, USA), -gamma-H2AX (1:1000) (Merck Millipore, Guyancourt, France) or p-ATM (1:1000) (Cell Signaling Technology, Danvers, MA, USA) primary antibodies, followed by horseradish peroxidase-conjugated anti-rabbit secondary antibodies (1:10,000; Sigma-Aldrich, Saint-Louis, MO, USA). GAPDH level was used to evaluate protein loading. Levels of protein expression were quantified using the G-Box system (Syngene; Cambridge UK).

2.7. Gamma-H2AX immunofluorescent measurement

For double strand breaks formation, 2 × 10^4 cells were grown on cover slip and were exposed for 2 days to 0 and 4 MBq/mL of ^{125}I-

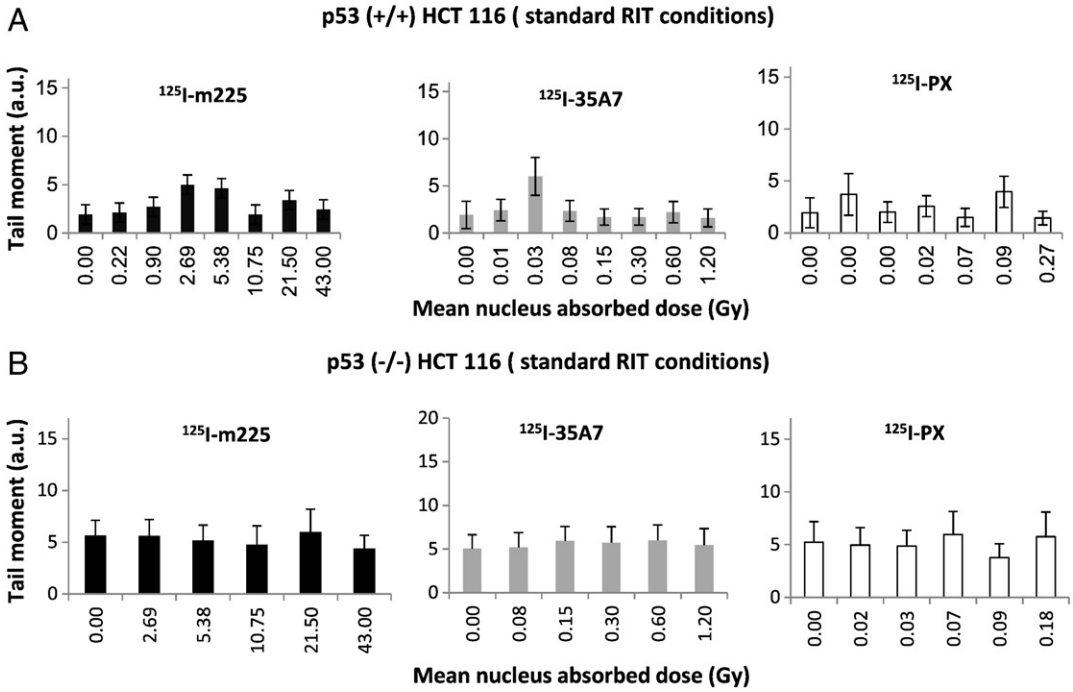

Fig. 1. DNA damage in $p53^{+/+}$ (panel A) and $p53^{-/-}$ (panel B) HCT116 cells after RIT at 37 °C. The alkaline comet assay was used to measure DNA damage at various time points (15 min and then 1, 2, 3, 6, 12, 24 and 48 h) in HCT116 cells targeted with 0 or 4 MBq/mL of internalizing anti-HER1 (m225), non-internalizing anti-CEA (35A7)) or non-targeting (PX) ^{125}I-mAbs at 37 °C (standard RIT conditions). The mean TM of 100 randomly chosen cells per slide was calculated using the Comet Imager 2.0 software. Three slides were analyzed per each condition and time point and experiments were repeated three times.

mAbs. Cells were washed twice with PBS and fixed in 3.7% formaldehyde in PBS for 30 min. They were then permeabilized at room temperature for 30 min using PBS/Triton (0.5%). Cells were next washed twice with PBS, saturated with PBS/BSA (1 mg/ml) for 1 hour before incubation overnight with anti-gamma-H2AX (1:200 PBS/BSA; Merck Millipore). Next, cover slips were incubated for 1 h in the dark with FITC-labeled goat anti-mouse Ig (Sigma) in PBS-BSA and next washed three times with PBS-BSA and once with PBS before analysis.

2.8. Cell cycle

20×10^4 HCT116 cells were grown in 6-well plates one day before RIT. Cells were harvested at day 0, 1, 2, 3, 4 and 7 of RIT by

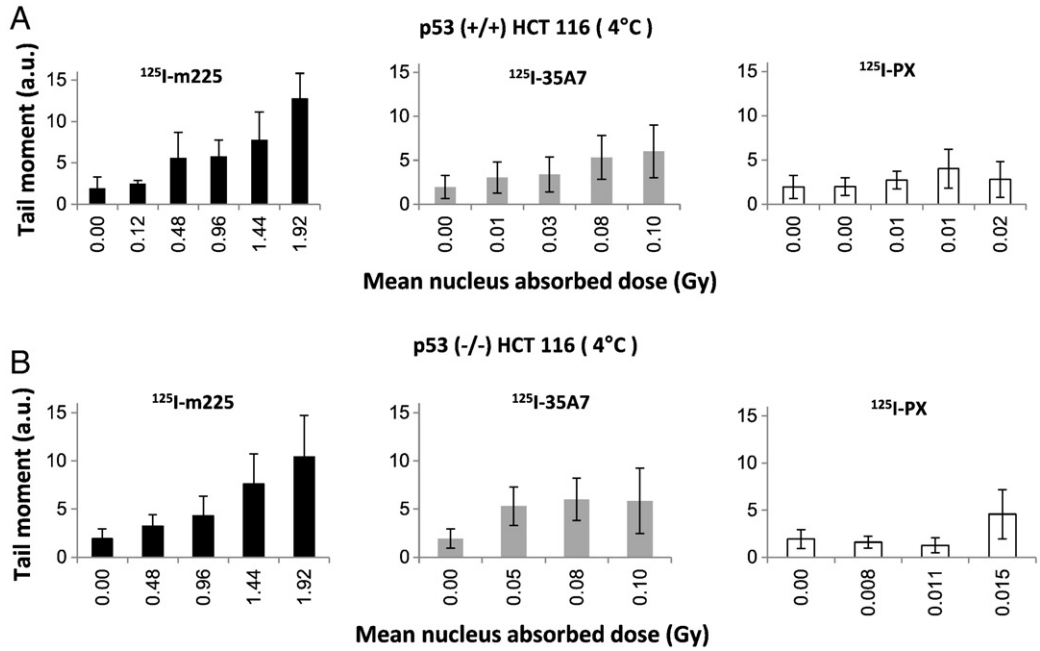

Fig. 2. DNA damage in $p53^{+/+}$ (panel A) and $p53^{-/-}$ (panel B) HCT116 after RIT at 4 °C. The alkaline comet assay was used to measure DNA damage at various time points (15 min, 30 min and then 1, 2, 3 and 4 h) in HCT116 cells exposed to 4 MBq/mL of internalizing anti-HER1 (m225), non-internalizing anti-CEA (35A7) or non-targeting (PX) ^{125}I-mAbs at 4 °C. TM was measured as a function of the mean nucleus absorbed dose, but only during 4 hours in order to keep cells alive. The mean TM of 100 randomly chosen cells per slide was calculated using the Comet Imager 2.0 software. Three slides were analyzed per each condition and time point and experiments were repeated three times.

trypsinization and washed twice with PBS. They were then fixed in 70% ethanol at−20 °C for 3 hours and stained with cell cycle kit reagent from Merck Millipore (Merck Millipore, Guyancourt, France) in the dark for 30 min at room temperature before analysis using an Muse® flow cytometer (Merck Millipore, Guyancourt, France). The percentage of cells in G0/G1, S and G2/M phases was then calculated (mean of three experiments in triplicate).

2.9. Statistical analysis

The linear mixed regression model (LMRM) [20] was used for statistical analysis of the data.

3. Results

3.1. DNA damage formation and repair occur simultaneously during RIT

We investigated the occurrence of DNA single (SSBs) and double (DSBs) strand breaks and alkali-labile sites (ALSs) in $p53^{+/+}$ and $p53^{-/-}$ HCT116 cells upon exposure to 4 MBq/mL of anti-CEA (35A7), anti-HER1 (m225) or non-targeting (PX) ^{125}I-mAbs for 2 days. The mean nucleus doses were calculated [19] using the MIRD cellular formalism. Under standard RIT conditions (at 37 °C), occurrence of DNA damage (as indicated by the TM parameter) was not significantly different in HCT116 cells treated with anti-HER1 or anti-CEA ^{125}I-mAbs in comparison to untreated cells ($p = 0.85$ and $p = 0.72$, respectively) (Fig. 1).

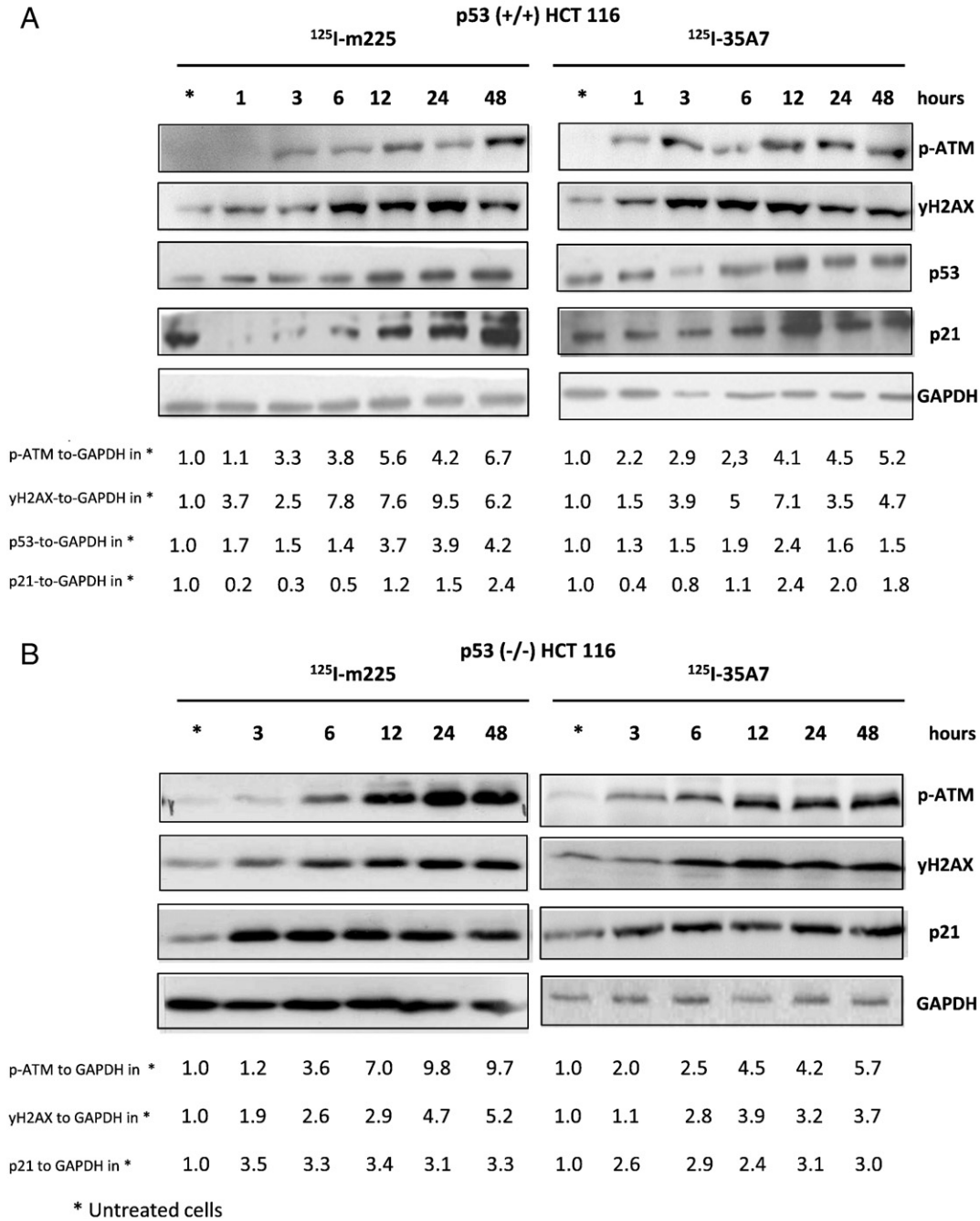

Fig. 3. Activation of DNA damage-related signaling proteins. The level of phosphorylated ATM (p-ATM) and H2AX (gamma-H2AX), p53 and p21 proteins was measured at the indicated time points in HCT116 cells exposed to 0 and 4 MBq/mL of internalizing anti-HER1 (m225), non-internalizing anti-CEA (35A7) ^{125}I-mAbs. GAPDH served as loading control (bottom). Panel A: $p53^{+/+}$ HCT116 cells and panel B: $p53^{-/-}$ HCT116 cells.

This finding suggests that radiation-induced DNA damage formation was compensated by DNA repair during RIT. In order to confirm this hypothesis, we investigated the level of DNA breaks in cells incubated with ^{125}I-mAbs at 4 °C for 4 h (instead of 48 h at 37 °C as used under standard RIT). Temperature of 4 °C is known to block enzymatic systems involved in DNA breaks repair. The 4 h exposure time was determined as the longest time of exposure at 4 °C producing no cytotoxicity. We observed under these conditions a progressive increase in DNA damage in $p53^{+/+}$ and $p53^{-/-}$ HCT116 cells exposed to anti-CEA and anti-HER1 ^{125}I-mAbs in comparison to those treated with non-targeting ^{125}I-mAbs (Fig. 2A and B). These data confirmed that DNA repair occurred during standard RIT while DNA breaks accumulated at 4 °C. We next calculated, the corresponding absorbed doses delivered to the nucleus by 4 MBq/mL ^{125}I-mAbs. We thus considered the cumulative number of decays ($\tilde{A}_{rs}$) calculated over 4 h (and not 48 h like under standard RIT). We also considered that internalization of mAbs was blocked at 4 °C such that *S*-values for cell surface localization were used for internalizing mAbs. Absorbed doses were then shown to be lower than under standard RIT (anti-HER1 ^{125}I-mAbs: from 43 Gy at 37 °C to 1.92 Gy at 4 °C; anti-CEA ^{125}I-mAbs: from 1.20 Gy to 0.1 Gy; non-targeting ^{125}I-mAbs from 0.27 Gy to 0.015). Corresponding highest TM values were 12.8 (anti-HER1 ^{125}I-mAbs), 6.0 (anti-CEA ^{125}I-mAbs) and 2.8 (non-targeting ^{125}I-mAbs) a.u. in $p53^{+/+}$ HCT116 cells and 10.4 (anti-HER1 ^{125}I-mAbs), 5.9 (anti-CEA ^{125}I-mAbs) and 4.5 (non-targeting ^{125}I-mAbs) a.u. in $p53^{-/-}$ cells. In cells exposed to anti-HER1 ^{125}I-mAbs, TM increased linearly as a function of the absorbed dose in both $p53^{+/+}$ and $p53^{-/-}$ HCT116 cells ($p < 0.001$). Following exposure to anti-CEA ^{125}I-mAbs, TM increase was linear in $p53^{+/+}$ HCT116 cells ($p < 0.007$), but not in $p53^{-/-}$ cells ($p = 0.103$), where it exhibited a larger standard error (Fig. 2A and B). However, comparison of the efficacy of anti-CEA and anti-HER1 ^{125}I-mAbs showed that, overall, they produced quantitatively similar effects in both $p53^{-/-}$ ($p = 0.251$) and $p53^{+/+}$ ($p = 0.172$) HCT116 cells, because anti-CEA ^{125}I-mAbs (with lower mean nucleus absorbed doses) were more efficient per Gy than anti-HER1 ^{125}I-mAbs (with higher mean absorbed doses) in producing DNA damage. Moreover, the effect of each antibody was similar in the two cell lines ($p = 0.681$ for anti-CEA ^{125}I-mAbs and $p = 0.372$ for anti-HER1 ^{125}I-mAbs).

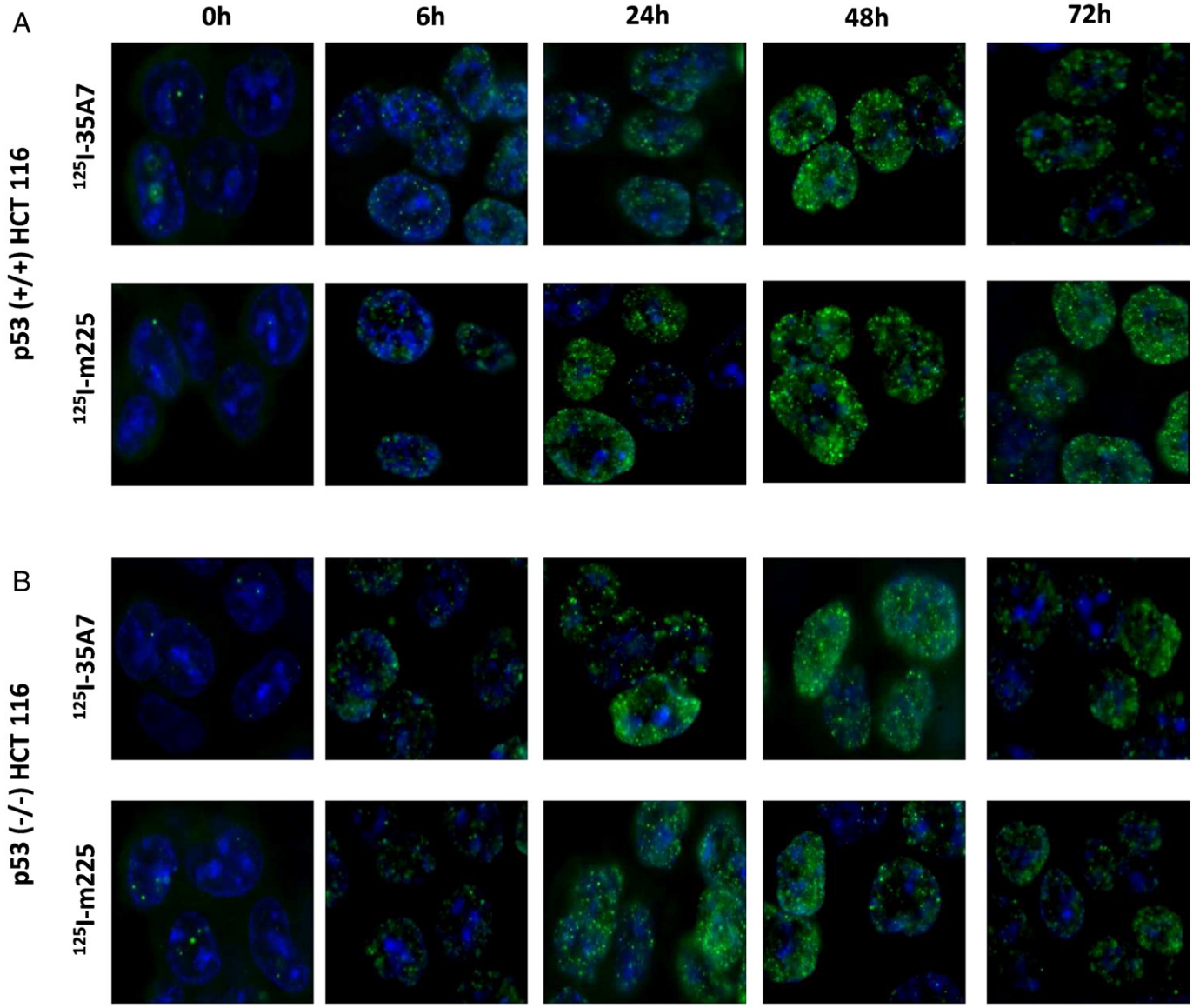

Fig.4. Immunofluorescent detection of gamma-H2AX in cells. Cells were grown on cover slip and exposed for 2 days to 0 and 4 MBq/mL of ^{125}I-mAbs. Gamma-H2AX foci were next detected at various time in (A) $p53^{+/+}$ and (B) $p53^{-/-}$ following onset of exposure to ^{125}I-mAbs.

3.2. DNA damage-mediated signaling pathways are efficiently activated in HCT116 cells

Under standard RIT conditions, the comet assay results suggested activation of DNA repair mechanisms. We thus assessed whether such low levels of RIT-induced DNA damage could activate ATM, H2AX and p53 (one of the key proteins of the radiation response) (Fig. 3). Western blot analysis revealed that phosphorylated ATM (p-ATM) and p53 level increased in $p53^{+/+}$ HCT116 cells exposed to RIT at 37 °C and were associated with p21 up-regulation (Fig. 3A). The extent of their induction was not correlated with the nucleus absorbed dose because it was only slightly higher upon exposure to anti-HER1 ^{125}I-mAbs than to anti-CEA ^{125}I-mAbs, although much different doses were delivered to the nucleus (43 Gy versus 1.2 Gy). Detection of gamma-H2AX indicated that DNA DSBs were continuously produced under standard RIT conditions (Fig. 3A), while no increase could be observed using the comet assay which detects all kind of breaks (DSBs + SSBs + ALSs). Similar results were obtained in $p53^{-/-}$ HCT116 cells for p-ATM, gamma-H2AX, and p21 (Fig. 3B).

Activation of p53 was also observed in A-431 ($p53^{+/+}$), but not in SK-OV-3 ($p53^{-/-}$) cells exposed to ^{125}I-mAbs (Supplementary Fig. 1). These two cell lines are more sensitive to non-internalizing anti-CEA than to internalizing anti-HER1/HER2 ^{125}I-mAbs [20]. In HCT116 and A-431 cells, p53 up-regulation is followed by induction of apoptosis at day 2 post-RIT [19]. These results suggest that the DNA damage induced by mean nucleus absorbed doses as low as 1.2 Gy can be efficiently detected in cells exposed to RIT.

The p21 protein up-regulation measured in HCT 116 cells was accompanied by cell cycle arrest in G2/M phase in both $p53^{+/+}$ and $p53^{-/-}$ cells upon exposure to anti-CEA and anti–HER1 ^{125}I-mAbs (Fig. 6). In both cell lines, the % of cells in G2/M was shown to increase significantly at day 1 post onset of RIT up to day 7.

3.3. Double strand breaks detection

Double strand breaks (DSBs) as revealed by gamma-H2AX foci detection were produced in $p53^{-/-}$ and $p53^{+/+}$ HCT 116 cells exposed for 2 days to 4 MBq/mL of either internalizing anti-HER1 or non-internalizing anti-CEA ^{125}I-mAbs (Fig. 4). DSBs were detected as early as 6 h post incubation with radiolabeled mAbs and their yield was continuously increasing in a similar way for both types of mAbs, independently of the mean nucleus absorbed dose. Moreover, they were still detected 24 h after the radioactivity was removed, namely 72 h post onset of RIT. These data suggest that DSBs are continuously formed under RIT using ^{125}I-mAbs and that they are not accurately repaired and accumulate with time.

3.4. Yield of micronuclei as a function of the mean nucleus absorbed dose

Micronuclei per binucleated cells (MN/BN) were produced in both $p53^{+/+}$ and $p53^{-/-}$ HCT116 cells during RIT using ^{125}I-mAbs, suggesting error-prone DNA repair. In $p53^{+/+}$ HCT116 cells, their formation at 24 h post onset of RIT using either internalizing anti-HER1 or non-internalizing anti-CEA ^{125}I-mAbs was increasing with the test activity. For non-internalizing ^{125}I-mAbs, yield of MN at 4 MBq/mL was higher at 24 h (0.34 ± 0.06 MN/BN versus 0.14 ±0.06 MN/BN at 0 MBq/mL) than at 48 h (0.20 ± 0.11 MN/BN) and it decreased to background level at 72 h (0.12 ± 0.08). Similar

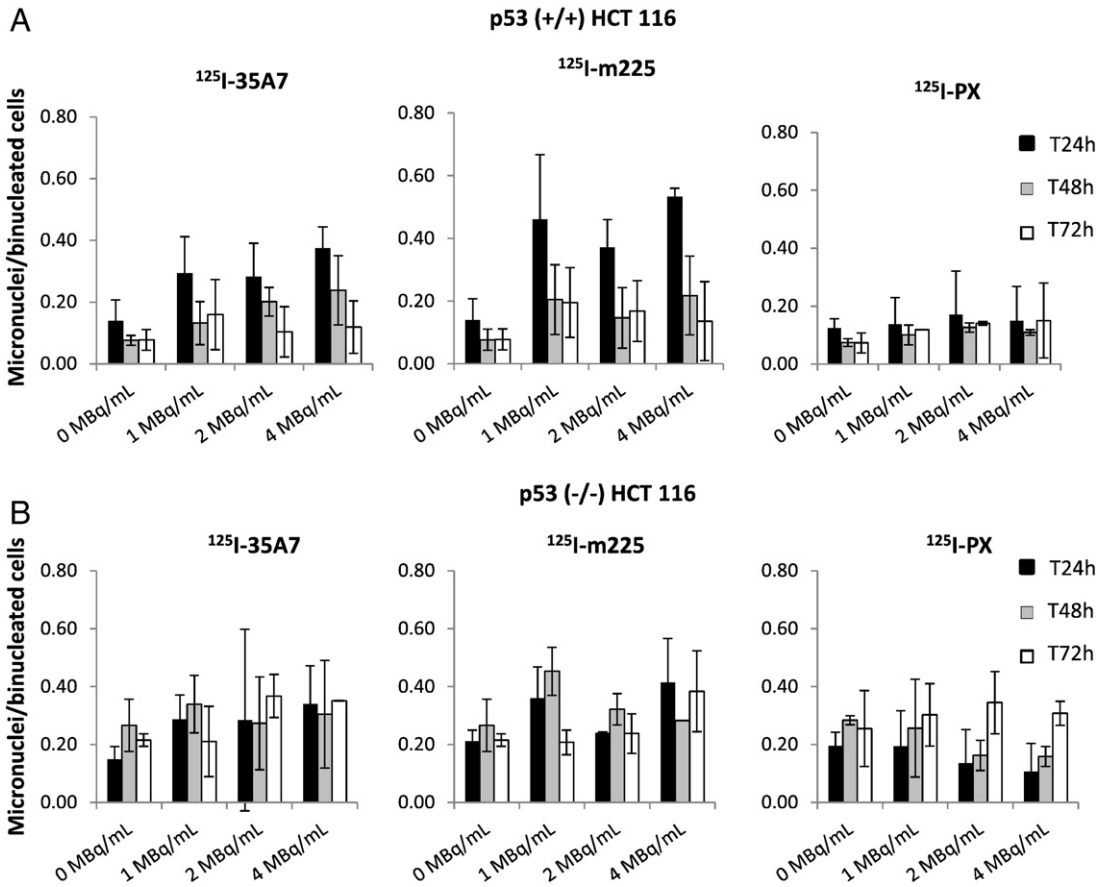

Fig. 5. Micronucleus (MN) frequency. $p53^{+/+}$ (panel A) and $p53^{-/-}$ (panel B) HCT116 cells were exposed to 0, 1, 2 and 4 MBq/mL of internalizing anti-HER1 (m225), non-internalizing anti-CEA (35A7) or non-targeting (PX) ^{125}I-mAbs. Micronuclei (MN) occurrence was determined in 500 binucleated cells at day 1, 2 and 3 of incubation and the cumulative MN frequency during the three days was determined.

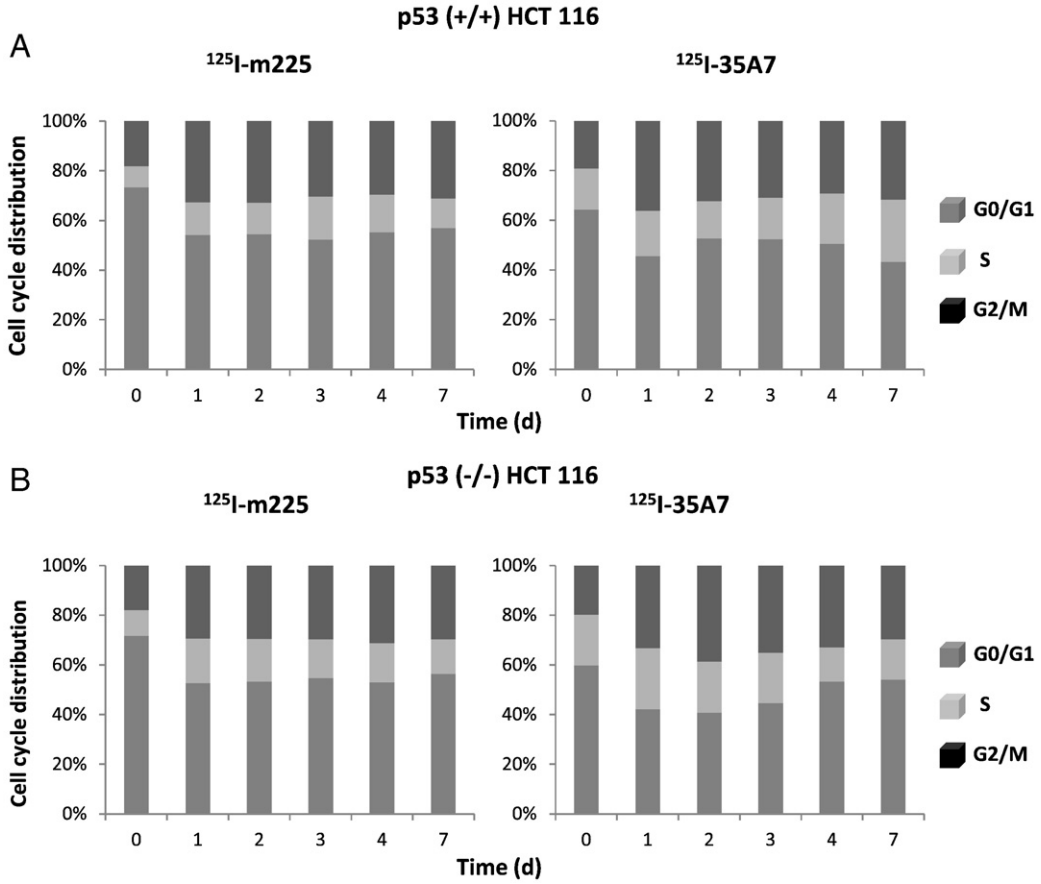

Fig. 6. Cell cycle analysis. $p53^{+/+}$ (panel A) and $p53^{-/-}$ (panel B) HCT116 cells were exposed to 0 or 4 MBq/mL of internalizing anti-HER1 (m225), non-internalizing anti-CEA (35A7) for several days. Cells were collected at day 0, 1, 2, 3, 4 and 7 of RIT, fixed in 70% ethanol for 3 hours and stained with Cell Cycle Kit reagent for analysis by flow cytometry. Experiments were repeated in triplicate.

observation could be done with internalizing ^{125}I-mAbs (0.53 ± 0.02 MN/BN at 24 h, 0.22 ± 0.04 MN/BN at 48 h, 0.14 ± 0.12 MN/BN at 72 h). It must be noted that yield of MN/BN in cells treated with non-specific ^{125}I-PX mAbs remained at the background level (between 0.08 ± 0.03 and 0.14 ± 0.06MN/BN).

In $p53^{-/-}$ HCT116 cells, relationship between MN yield and test activity was less pronounced (Fig. 5). This can be partly due to a higher background level in non-treated cells (around between 0.15 and 0.27MN/BN) and to large uncertainties associated to MN measurement. Similarly, no clear trend of a decrease between 24 h and 48 h in MN yield was observed.

4. Discussion

We showed previously in HCT116 cells targeted by 4 MBq/mL of ^{125}I-mAbs (Fig. 7 and Ref. [19]) that a mean nucleus absorbed dose of 1.2 Gy of non-internalizing anti-CEA ^{125}I-mAbs is as effective as 43 Gy of internalizing anti-HER1 ^{125}I-mAbs. As the cell response to ionizing radiation is generally, in CEBRT, triggered by nuclear DNA damage, we thus investigated the relationship between the energy deposited in the nucleus (i.e., the mean nucleus absorbed dose) and several biological endpoints during RIT with ^{125}I-mAbs. Non-internalizing anti-CEA ^{125}I-mAbs and, to a lower extent, internalizing anti-HER1 ^{125}I-mAbs, were very efficient in killing cells [19] and also in producing DNA damage despite lower dose-rates (about 0.025 Gy.h^{-1} for anti-CEA ^{125}I-mAbs and 0.9 Gy.h^{-1} for anti-HER1 ^{125}I-mAbs) than in CEBRT (about 2 Gy.min^{-1}). The high efficiency of ^{125}I-mAbs, particularly of anti-CEA ^{125}I-mAbs per unit-dose, is reminiscent of low-dose hyper-radiosensitivity and of the inverse dose-rate effect. These two phenomena, which were reported in CEBRT (for review [32]) after low dose (below 0.5 Gy) or low dose-rate (0.02–1.00 Gy.h^{-1}) exposure, lead to increased effectiveness of radiation per unit-dose beyond what could be predicted by the conventional linear and linear quadratic radio-biologic models ([33] and for review [32]). It has been proposed that they are the result of decreased sensing of DNA damage by signaling proteins and of the consequent reduced activation of the early DNA damage response through ATM and p53 or the G2 checkpoint ([34] and for review [29]). Our findings do not support this hypothesis. Indeed, ATM, H2AX and p21 were efficiently activated in $p53^{-/-}$ and $p53^{+/+}$ HCT116 cells and p53 expression was also increased (in $p53^{+/+}$ HCT116 cells and A-431 cells) during RIT with ^{125}I-mAbs. Moreover, most of the DNA breaks were immediately repaired under standard RIT conditions (comet assay data, Figs. 1 and 2). However, the significant increase in expression and accumulation of gamma-H2AX, due to phosphorylation of H2AX at DSB sites [35] in cells treated with anti-CEA or anti-HER1 ^{125}I-mAbs indicates that DSBs were continuously formed and not repaired. Consequently, mis- or un-repaired DSBs might have led to micronuclei formation (Fig. 4) and to mitotic death of damaged cells. These data indicate that acute cell death associated with low doses and low dose-rate of ^{125}I-mAbs (particularly of non-internalizing anti-CEA ^{125}I-mAbs) was not due to defective detection of DNA damage by the cells. Impaired repair of double strand breaks would be involved in low dose rate efficacy of RIT using ^{125}I-mAbs in a non-dependent dose-effect relationship.

Another intriguing observation is the lack of relationship between the mean nucleus absorbed doses (in Gy) and these biological endpoints when comparing the efficacy/Gy of anti-CEA and anti-HER1 ^{125}I-mAbs. In CEBRT, the biological effects and, consequently,

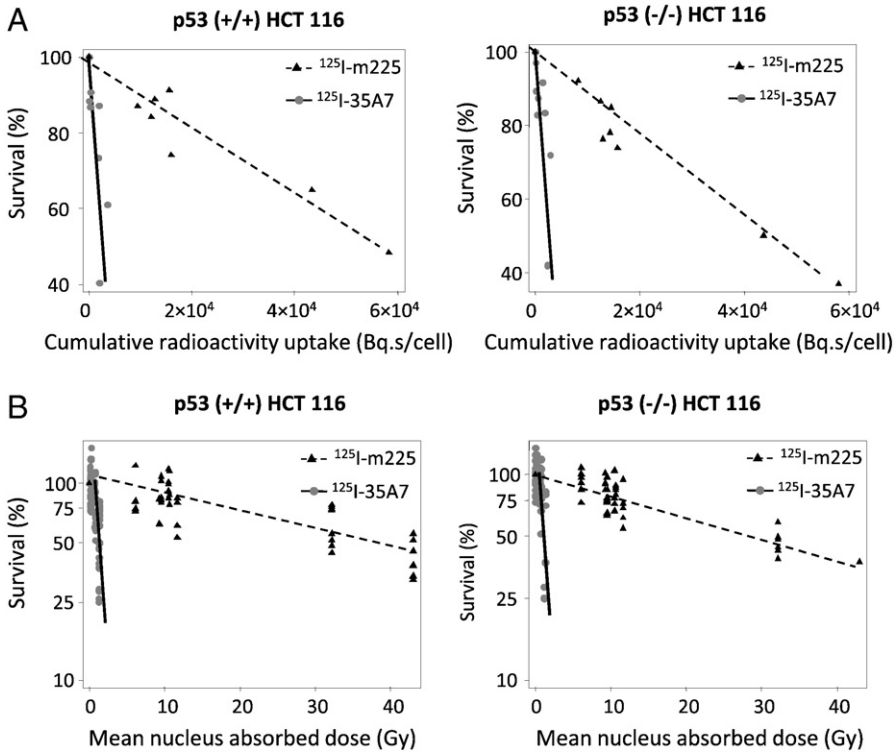

Fig. 7. Survival. Clonogenic survival was assessed in (A) $p53^{+/+}$ and (B) $p53^{-/-}$ HCT116 cells following exposure to test activities of ^{125}I-mAbs that gradually increased from 0 to 4 MBq/mL for 2 days. Cells were targeted with internalizing anti-HER1 (m225), non-internalizing anti-CEA (35A7) ^{125}I-mAbs. Survival was expressed as a function of (A) the total cumulative radioactivity uptake $\tilde{A}_{rs}$ (B) the mean nucleus absorbed dose. Results are the mean of four experiments done in triplicate (from Paillas et al. [19]).

the survival of irradiated cells are correlated with the mean nucleus absorbed dose [36], according to a linear or linear quadratic relationship depending on whether low-LET or high-LET radiations are used. Here, no linear dose-effect relationship was observed when the effects per Gy of absorbed dose of anti-CEA and anti-HER1 ^{125}I-mAbs are considered. Indeed, the biological response per Gy of non-internalizing anti-CEA ^{125}I-mAbs was much higher than that of internalizing anti-HER1 ^{125}I-mAbs. Hence, quantitatively similar effects were produced by ^{125}I-mAbs with much different nucleus absorbed doses. This is true for clonogenic survival [27], frequency of DNA breaks and micronuclei formation, induction of DNA damage response and effects on cell cycle progression. Based on the localization of the energy deposits due to decay of anti-CEA ^{125}I-mAbs at the cell membrane [19] and the lack of correlation between absorbed dose and biological effects we hypothesize that cell membrane-mediated ^{125}I-induced bystander effect, as described in CEBRT ([37–39] and for reviews [29,40]), could play a significant role in the higher efficacy of non-internalizing ^{125}I-mAbs [41–43] and should be further investigated.

We would like to highlight that the hypersensitivity of HCT116 cells to non-internalizing ^{125}I-mAbs is not dependent on our dosimetric approach based on MIRD formalism since we showed that it was still observed when survival was expressed as a function of cumulated uptake of radioactivity (Fig. 7A). Moreover, cytoplasmic and cell surface localizations of m225 and 35A7, respectively, were confirmed in several cell lines using cell fractionation assays and immunofluorescence approaches (unpublished data). However, it must be kept in mind that Bousis et al. showed that for the case where the radiopharmaceutical are either internalized into the cytoplasm or remained bound onto the cell surface (non-internalized), the dose to the cell nucleus determined using Monte Carlo code was found to differ significantly from the MIRD values. Then, use of MIRD formalism with short range Auger electrons emitters must be done carefully [44].

In conclusion, this study shows that DNA damage produced by low dose of ^{125}I-mAbs is efficiently detected by targeted cells even after very low absorbed dose, but is associated to accumulation of DNA double strand breaks. G2/M cell cycle arrest does not prevent damaged cells still proceed through cell cycle and to undergo mitotic death. The lack of dose-effect relationship between mean nucleus absorbed dose and several biological endpoints and the property of non-internalizing ^{125}I-mAbs to deliver localized doses at the cell membrane suggest that cell membrane-mediated bystander effects might be involved in ^{125}I-mAbs cytotoxicity.

Supplementary data to this article can be found online at http://dx.doi.org/10.1016/j.nucmedbio.2014.01.012.

Acknowledgment

This work was supported by the Institut National du Cancer, grant R09080FF/RPT09005FFA and by Action Nu1.1 of Plan Cancer 2009–2013 (ASC 13038FSA).

References

[1] Pomplun E, Booz J, Charlton DE. A Monte Carlo simulation of Auger cascades. Radiat Res 1987;111(3):533–52.
[2] Buchegger F, Perillo-Adamer F, Dupertuis YM, Delaloye AB. Auger radiation targeted into DNA: a therapy perspective. Eur J Nucl Med Mol Imaging 2006;33(11):1352–63.
[3] Howell RW. Auger processes in the 21st century. Int J Radiat Biol 2008;84(12):959–75.
[4] Kassis AI. Radiotargeting agents for cancer therapy. Expert Opin Drug Deliv 2005;2(6):981–91.
[5] Cornelissen B, Vallis KA. Targeting the nucleus: an overview of Auger-electron radionuclide therapy. Curr Drug Discov Technol 2010;7(4):263–79.
[6] Pomplun E. Auger electron spectra – the basic data for understanding the Auger effect. Acta Oncol 2000;39(6):673–9.
[7] Yasui LS. Molecular and cellular effects of Auger emitters: 2008–2011. Int J Radiat Biol; 2012.
[8] Feinendegen LE. The Auger effect in biology and medicine. Looking back. Int J Radiat Biol 2012;88(12):862–3.

[9] Li L, Quang TS, Gracely EJ, Kim JH, Emrich JG, Yaeger TE, et al. A Phase II study of anti-epidermal growth factor receptor radioimmunotherapy in the treatment of glioblastoma multiforme. J Neurosurg 2010;113(2):192–8.
[10] Quang TS, Brady LW. Radioimmunotherapy as a novel treatment regimen: 125I-labeled monoclonal antibody 425 in the treatment of high-grade brain gliomas. Int J Radiat Oncol Biol Phys 2004;58(3):972–5.
[11] Welt S, Divgi CR, Real FX, Yeh SD, Garin-Chesa P, Finstad CL, et al. Quantitative analysis of antibody localization in human metastatic colon cancer: a phase I study of monoclonal antibody A33. J Clin Oncol 1990;8(11):1894–906.
[12] Welt S, Scott AM, Divgi CR, Kemeny NE, Finn RD, Daghighian F, et al. Phase I/II study of iodine 125-labeled monoclonal antibody A33 in patients with advanced colon cancer. J Clin Oncol 1996;14(6):1787–97.
[13] Santoro L, Boutaleb S, Garambois V, Bascoul-Mollevi C, Boudousq V, Kotzki PO, et al. Noninternalizing monoclonal antibodies are suitable candidates for 125I radioimmunotherapy of small-volume peritoneal carcinomatosis. J Nucl Med 2009;50(12):2033–41.
[14] Boudousq V, Ricaud S, Garambois V, Bascoul-Mollevi C, Boutaleb S, Busson M, et al. Brief intraperitoneal radioimmunotherapy of small peritoneal carcinomatosis using high activities of noninternalizing 125I-labeled monoclonal antibodies. J Nucl Med 2010;51(11):1748–55.
[15] Behr TM, Behe M, Lohr M, Sgouros G, Angerstein C, Wehrmann E, et al. Therapeutic advantages of Auger electron- over beta-emitting radiometals or radioiodine when conjugated to internalizing antibodies. Eur J Nucl Med 2000;27(7):753–65.
[16] Behr TM, Sgouros G, Vougiokas V, Memtsoudis S, Gratz S, Schmidberger H, et al. Therapeutic efficacy and dose-limiting toxicity of Auger-electron vs. beta emitters in radioimmunotherapy with internalizing antibodies: evaluation of 125I- vs. 131I-labeled CO17-1A in a human colorectal cancer model. Int J Cancer 1998;76(5):738–48.
[17] Michel RB, Brechbiel MW, Mattes MJ. A comparison of 4 radionuclides conjugated to antibodies for single-cell kill. J Nucl Med 2003;44(4):632–40.
[18] Govindan SV, Goldenberg DM, Elsamra SE, Griffiths GL, Ong GL, Brechbiel MW, et al. Radionuclides linked to a CD74 antibody as therapeutic agents for B-cell lymphoma: comparison of Auger electron emitters with beta-particle emitters. J Nucl Med 2000;41(12):2089–97.
[19] Paillas S, Boudousq V, Piron B, Kersual N, Chouin N, Mollevi C, et al. Apoptosis and p53 are not involved in the anti-tumor efficacy of 125I-labeled monoclonal antibodies targeting the cell membrane. Nucl Med Biol 2013;40:471–80.
[20] Pouget JP, Santoro L, Raymond L, Chouin N, Bardies M, Bascoul-Mollevi C, et al. Cell membrane is a more sensitive target than cytoplasm to dense ionization produced by auger electrons. Radiat Res 2008;170(2):192–200.
[21] Goodhead DT. Initial events in the cellular effects of ionizing radiations: clustered damage in DNA. Int J Radiat Biol 1994;65(1):7–17.
[22] Goodhead DT, Nikjoo H. Track structure analysis of ultrasoft X-rays compared to high- and low-LET radiations. Int J Radiat Biol 1989;55(4):513–29.
[23] Levine AJ, Oren M. The first 30 years of p53: growing ever more complex. Nat Rev Cancer 2009;9(10):749–58.
[24] Prise KM, Schettino G, Folkard M, Held KD. New insights on cell death from radiation exposure. Lancet Oncol 2005;6(7):520–8.
[25] O'Driscoll M, Jeggo PA. The role of double-strand break repair – insights from human genetics. Nat Rev Genet 2006;7(1):45–54.
[26] Meek DW. Tumour suppression by p53: a role for the DNA damage response? Nat Rev Cancer 2009;9(10):714–23.
[27] Knox SJ, Goris ML, Wessels BW. Overview of animal studies comparing radioimmunotherapy with dose equivalent external beam irradiation. Radiother Oncol 1992;23(2):111–7.
[28] Williams JA, Edwards JA, Dillehay LE. Quantitative comparison of radiolabeled antibody therapy and external beam radiotherapy in the treatment of human glioma xenografts. Int J Radiat Oncol Biol Phys 1992;24(1):111–7.
[29] Sgouros G, Knox SJ, Joiner MC, Morgan WF, Kassis AI. MIRD continuing education: bystander and low dose-rate effects: are these relevant to radionuclide therapy? J Nucl Med 2007;48(10):1683–91.
[30] Goddu SM, Howell RW, Bouchet LG, Bolch WE, Rao DV. MIRD cellular S values: self-absorbed dose per unit cumulated activity for selected radionuclides and monoenergetic electron and alpha particle emitters incorporated into different cell compartments. Reston, VA: Society of Nuclear Medicine; 1997.
[31] Laurent C, Pouget JP, Voisin P. Modulation of DNA damage by pentoxifylline and alpha-tocopherol in skin fibroblasts exposed to gamma rays. Radiat Res 2005;164(1):63–72.
[32] Marples B, Collis SJ. Low-dose hyper-radiosensitivity: past, present, and future. Int J Radiat Oncol Biol Phys 2008;70(5):1310–8.
[33] Joiner MC, Johns H. Renal damage in the mouse: the response to very small doses per fraction. Radiat Res 1988;114(2):385–98.
[34] Xu B, Kim ST, Lim DS, Kastan MB. Two molecularly distinct G(2)/M checkpoints are induced by ionizing irradiation. Mol Cell Biol 2002;22(4):1049–59.
[35] Lobrich M, Shibata A, Beucher A, Fisher A, Ensminger M, Goodarzi AA, et al. gammaH2AX foci analysis for monitoring DNA double-strand break repair: strengths, limitations and optimization. Cell Cycle 2010;9(4):662–9.
[36] Puck TT, Morkovin D, Marcus PI, Cieciura SJ. Action of x-rays on mammalian cells. II. Survival curves of cells from normal human tissues. J Exp Med 1957;106(4):485–500.
[37] Azzam EI, de Toledo SM, Little JB. Oxidative metabolism, gap junctions and the ionizing radiation-induced bystander effect. Oncogene 2003;22(45):7050–7.
[38] Sowa Resat MB, Morgan WF. Radiation-induced genomic instability: a role for secreted soluble factors in communicating the radiation response to non-irradiated cells. J Cell Biochem 2004;92(5):1013–9.
[39] Mamlouk O, Balagurumoorthy P, Wang K, Adelstein SJ, Kassis AI. Bystander effect in tumor cells produced by iodine-125 labeled human lymphocytes. Int J Radiat Biol; 2012.
[40] Prise KM, O'Sullivan JM. Radiation-induced bystander signalling in cancer therapy. Nat Rev Cancer 2009;9(5):351–60.
[41] Boyd M, Ross SC, Dorrens J, Fullerton NE, Tan KW, Zalutsky MR, et al. Radiation-induced biologic bystander effect elicited in vitro by targeted radiopharmaceuticals labeled with alpha-, beta-, and Auger electron-emitting radionuclides. J Nucl Med 2006;47(6):1007–15.
[42] Chouin N, Bernardeau K, Bardies M, Faivre-Chauvet A, Bourgeois M, Apostolidis C, et al. Evidence of extranuclear cell sensitivity to alpha-particle radiation using a microdosimetric model. II. Application of the microdosimetric model to experimental results. Radiat Res 2009;171(6):664–73.
[43] Nagasawa H, Cremesti A, Kolesnick R, Fuks Z, Little JB. Involvement of membrane signaling in the bystander effect in irradiated cells. Cancer Res 2002;62(9):2531–4.
[44] Bousis C, Emfietzoglou D, Hadjidoukas P, Nikjoo H. Monte Carlo single-cell dosimetry of Auger-electron emitting radionuclides. Phys Med Biol 2010;55(9):2555–72.